Supporting Information

Photoinitiated Reactivity of a Thiolate-Ligated, Spin-Crossover Nonheme $\{FeNO\}^7$ Complex with Dioxygen

Alison C. McQuilken,[†] Hirotoshi Matsumura,[‡,#] Maximilian Dürr,[§] Alex M. Confer,[†] John P. Sheckelton,[†,⊥] Maxime A. Siegler,[†] Tyrel M. McQueen,[†,⊥,∥] Ivana Ivanović-Burmazović,[,§] Pierre Moënne-Loccoz,*[,‡] David P. Goldberg*[,†]*

[†]Department of Chemistry, The Johns Hopkins University, Baltimore, Maryland, 21218, United States

[‡]Oregon Health & Science University, Institute of Environmental Health, Portland, OR, 97239, United States

[§]Department of Chemistry and Pharmacy, University of Erlangen-Nürnberg, 91058, Erlangen, Germany

[⊥]Institute for Quantum Matter and Department of Physics and Astronomy, The Johns Hopkins University, Baltimore, Maryland, 21218, United States

[∥]Department of Materials Science and Engineering, The Johns Hopkins University, Baltimore, Maryland, 21218, United States

[#]Present address: Department of Life Science, Faculty and Graduate School of Engineering and Resource Science, Akita University, Akita 010-8502, Japan

X-Ray Crystallography. All reflection intensities for **2** were measured at 293(2) K using a SuperNova diffractometer (equipped with Atlas detector) with Cu *K*α radiation (λ = 1.54178 Å) under the program CrysAlisPro (Version 1.171.36.32 Agilent Technologies, 2013). The same program was used to refine the cell dimensions and for data reduction. The structure was solved with the program SHELXS-2013 (Sheldrick, 2013) and was refined on F^2 with SHELXL-2013 (Sheldrick, 2013). Analytical numeric absorption corrections based on a multifaceted crystal model were applied using CrysAlisPro (Version 1.171.36.32 Agilent Technologies, 2013). The temperature of the data collection was controlled using the system Cryojet (manufactured by Oxford Instruments). The H atoms were placed at calculated positions using the instructions AFIX 13, AFIX 23 or AFIX 43 with isotropic displacement parameters having values 1.2 times *U*eq of the attached C atoms.

Crystal Structure of 2. The structure of **2** is mostly ordered. The nitric oxide and the BF_4^- counterion are found to be disordered over two orientations, and the occupancy factors of the major components of the disorder refine to 0.66(4) and 0.556(6), respectively. Fw = 570.18, black block, 0.23 × 0.20 × 0.17 mm^3, orthorhombic, *Pbca* (no. 61), a = 11.72284(19), b = 14.8569(2), c = 28.5647(5) Å, V = 4974.97(14) $Å^3$, Z = 8, D_x = 1.523 g cm^{-3}, μ = 6.166 mm^{-1}, abs. corr. range: 0.367–0.497. 17073 Reflections were measured up to a resolution of $(\sin \theta/\lambda)_{max}$ = 0.62 $Å^{-1}$. 4886 Reflections were unique (R_{int} = 0.0321), of which 3830 were observed [$I > 2\sigma(I)$]. 390 Parameters were refined using 221 restraints. $R1/wR2$ [$I > 2\sigma(I)$]: 0.0490/0.1372. $R1/wR2$ [all refl.]: 0.0637/0.1496. S = 1.028. Residual electron density found between -0.56 and 0.60 e $Å^{-3}$.

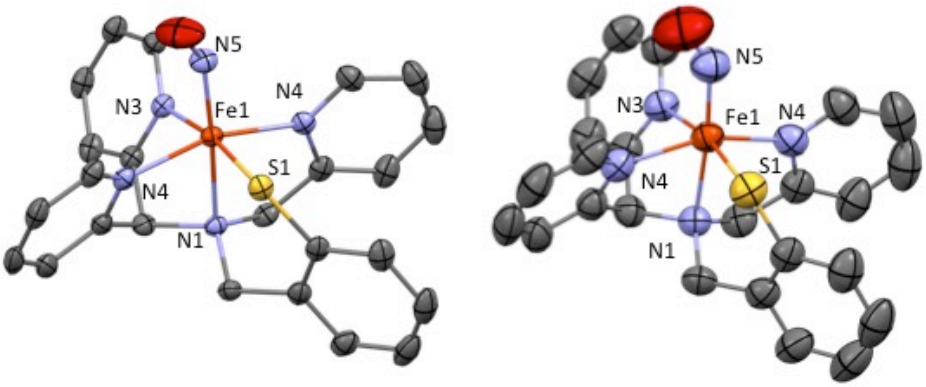

Figure S1. Displacement ellipsoid plots (50% probability level) of the cation of **2** determined at 110 K (left) and 293 K (right).

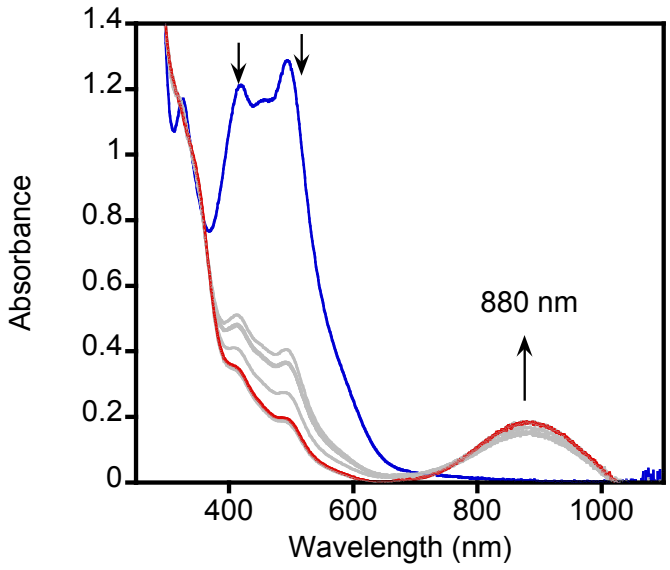

Figure S2. UV-vis spectra showing the generation of $[Fe^{III}(N3PyS)]^{2+}$ (red) upon addition of 1 equiv of $[FeCp_2]PF_6$ to **1** (blue) in CH_3CN under Ar.

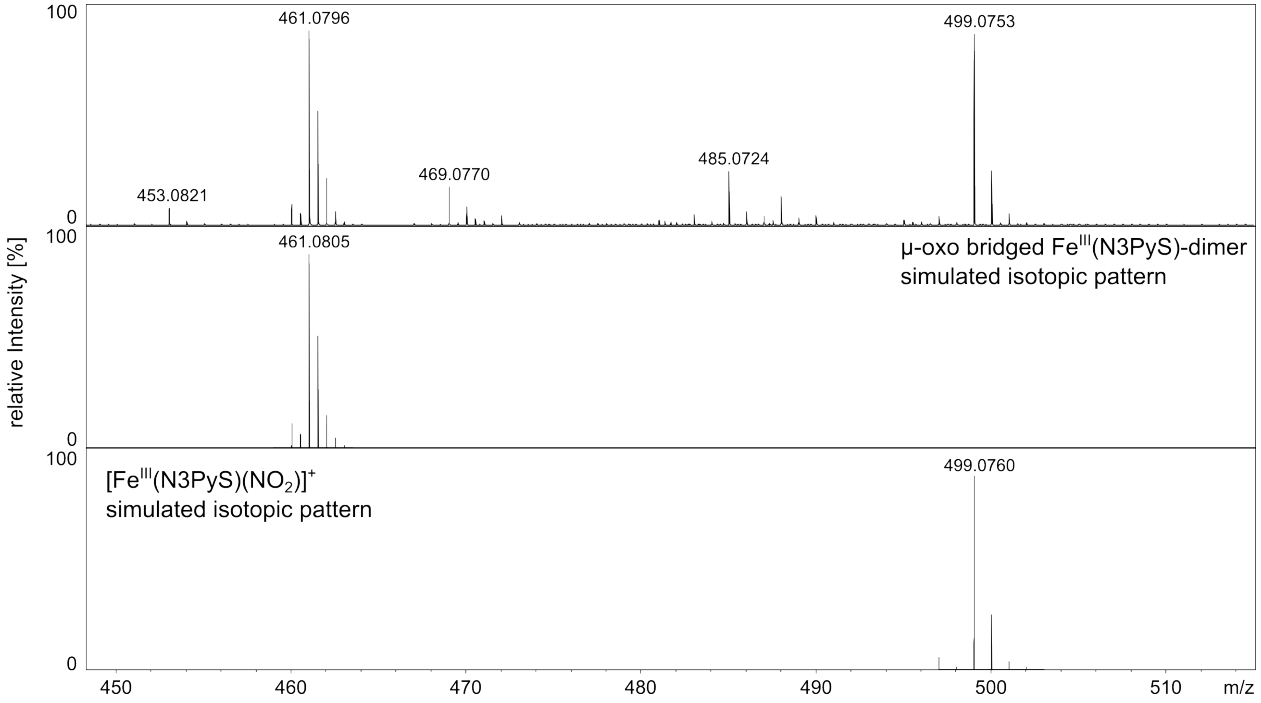

Figure S3. CSI-MS of a sample of **2** in CH_3CN after 10 min of photoirradiation (150 W xenon lamp: $\lambda > 400$ nm) in air (top spectrum) with simulated isotope patterns corresponding to $[(Fe^{III}(N3PyS))_2O]^{2+}$ (middle spectrum) and to $[Fe^{III}(NO_2)(N3PyS)]^+$ (bottom spectrum).

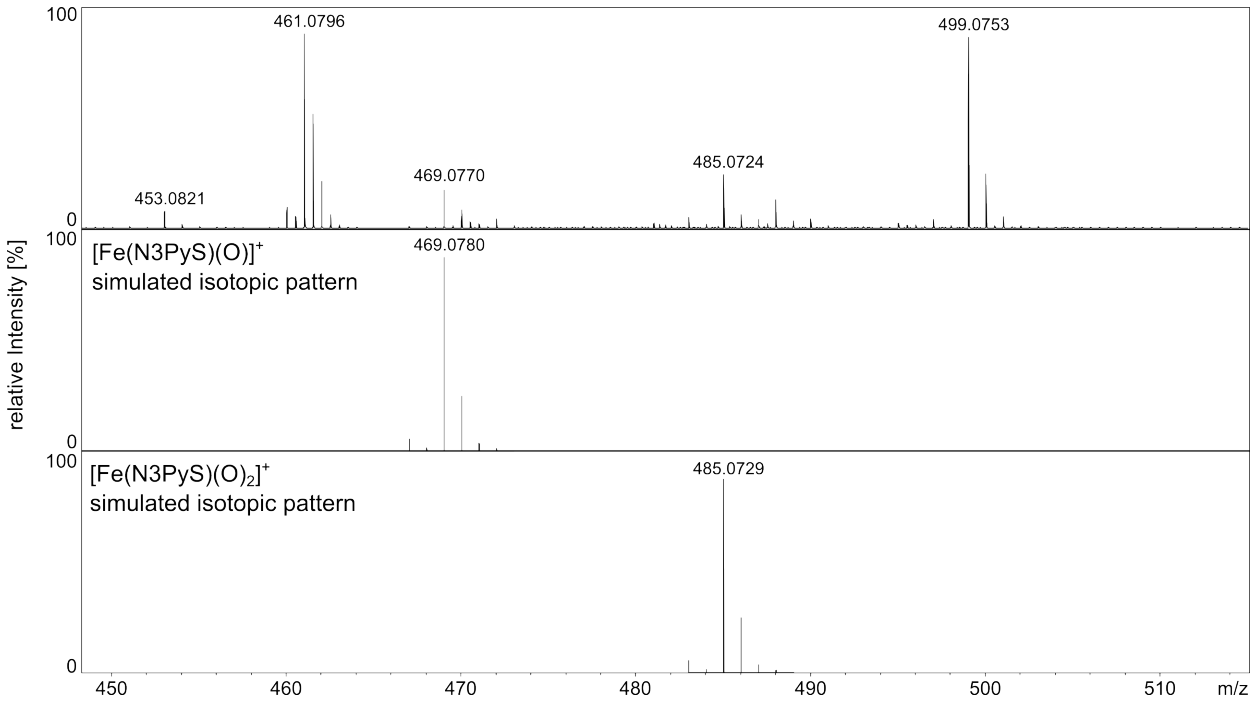

Figure S4. CSI-MS of a sample of **2** in CH_3CN after 10 min of photoirradiation (150 W xenon lamp: $\lambda > 400$ nm) in air (top spectrum) with simulated isotope patterns corresponding to $[Fe(N3PyS(O)]^+$ (middle spectrum) and to $[Fe(N3PyS(O)_2)]^+$ (bottom spectrum).

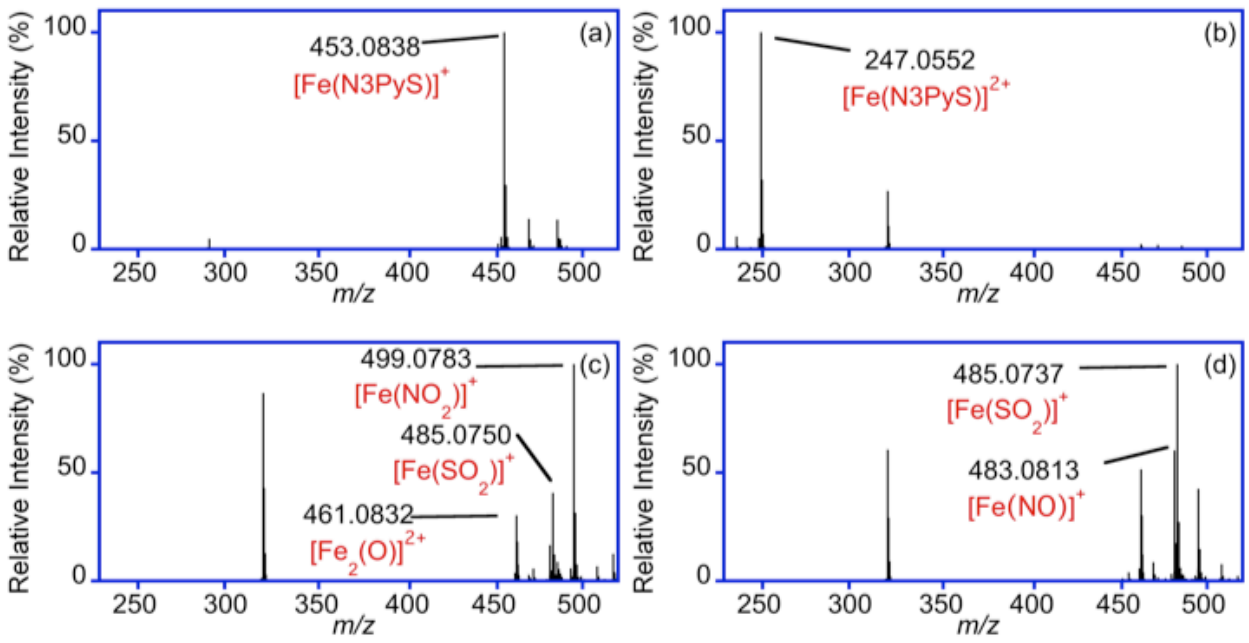

Figure S5. CSI-MS of the generation of **4** via Pathway B at 50 μM in CH_3CN; (a) **1**, (b) **1** + 1 equiv. $[FeCp_2]BF_4$, (c) **1** + $[FeCp_2]BF_4$ + Bu_4NNO_2 measured immediately upon mixing, and (d) measured after 20 min. The species at 311.081 is yet unidentified, however, the isotope pattern indicates it does not contain iron.

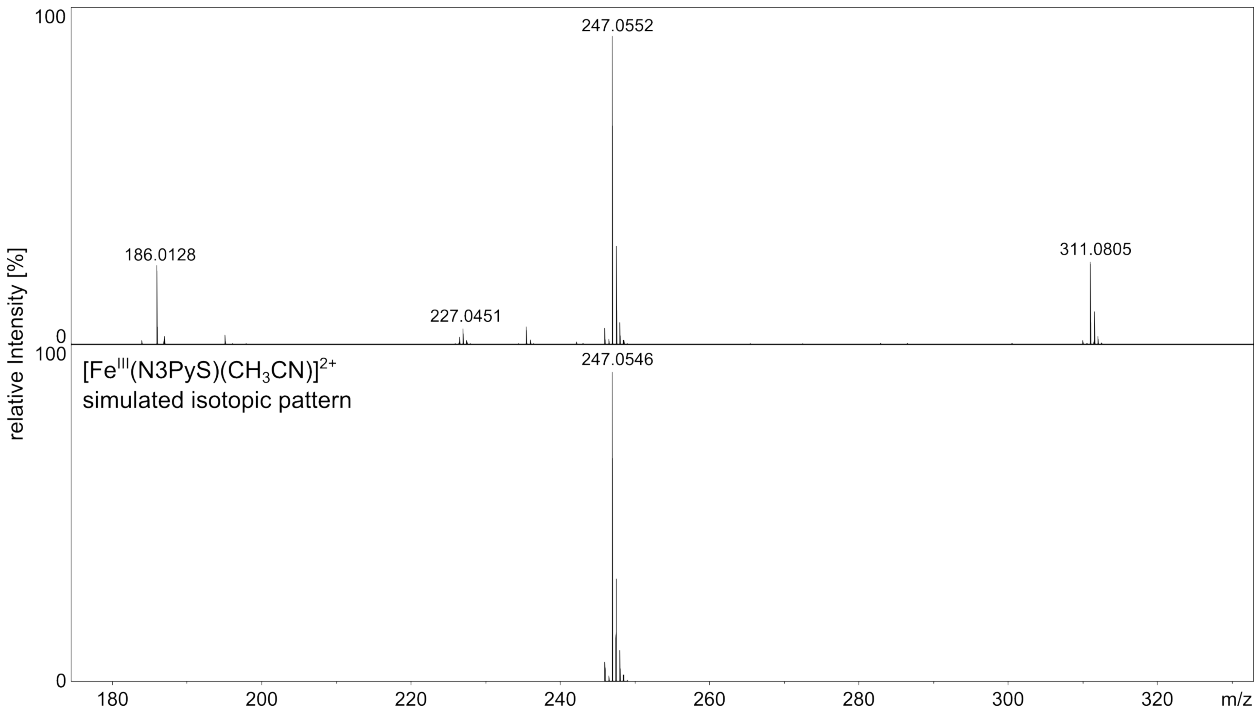

Figure S6. CSI-MS of a sample of **1** + 1 equiv. $[FeCp_2]BF_4$ (top spectrum) with the simulated isotope pattern corresponding to $[Fe^{III}(N3PyS)(CH_3CN)]^{2+}$ (bottom spectrum).

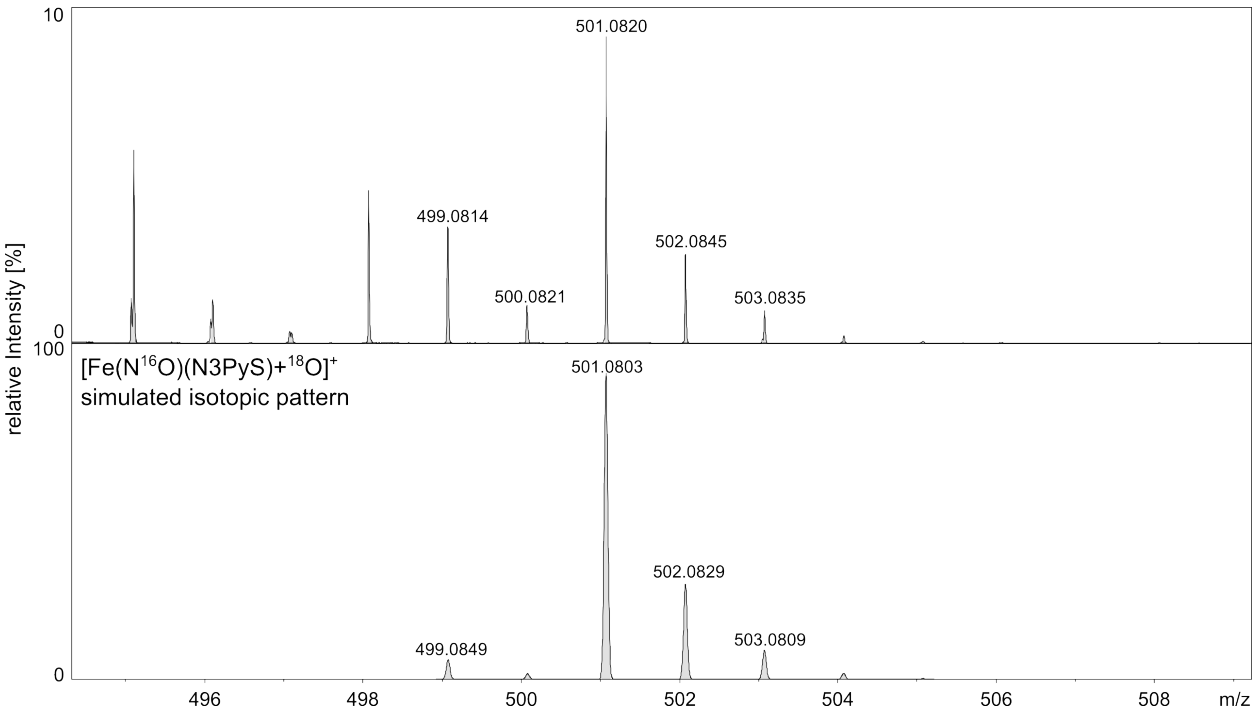

Figure S7. CSI-MS of a sample of **2** + $^{18}O_2$ in CH_3CN after 25 min of photoirradiation (150 W xenon lamp: $\lambda > 400$ nm) (top spectrum) with simulated isotope pattern corresponding to $[Fe(N^{16}O)(N3PyS)+^{18}O]^+$ (bottom spectrum).

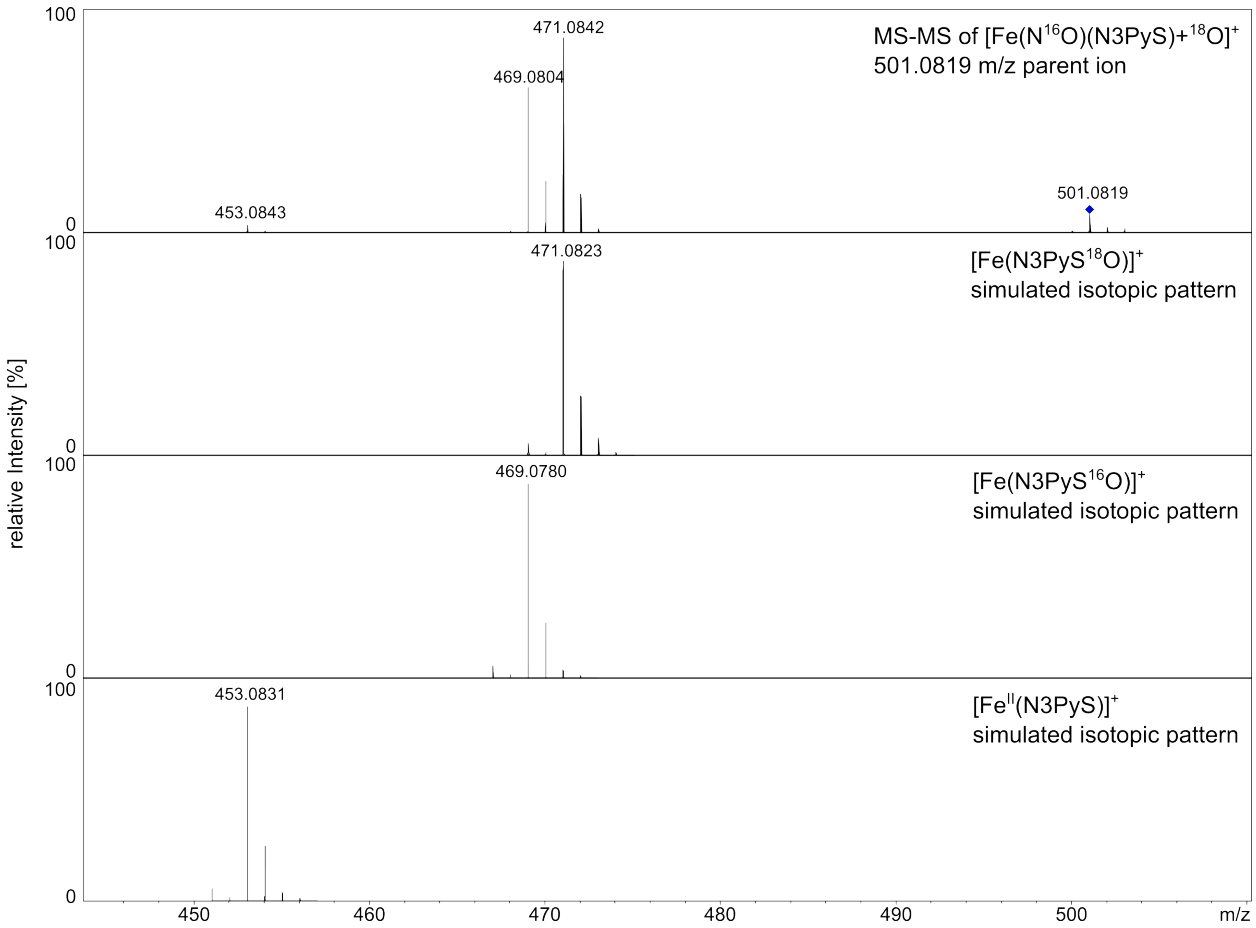

Figure S8. Tandem MS/MS of the parent ion at 501.0819 m/z (top spectrum) generated from the reaction of **2** + $^{18}O_2$ in CH_3CN after 25 min of photoirradiation, with the simulated isotope patterns corresponding to loss of NO• to give the sulfur-oxygenated products, $[Fe(N3PyS^{18}O)]^+$ (second spectrum) and $[Fe(N3PyS^{16}O)]^+$ (third spectrum), and to loss of NO_2• to give $[Fe^{II}(N3PyS)]^+$ (bottom spectrum).

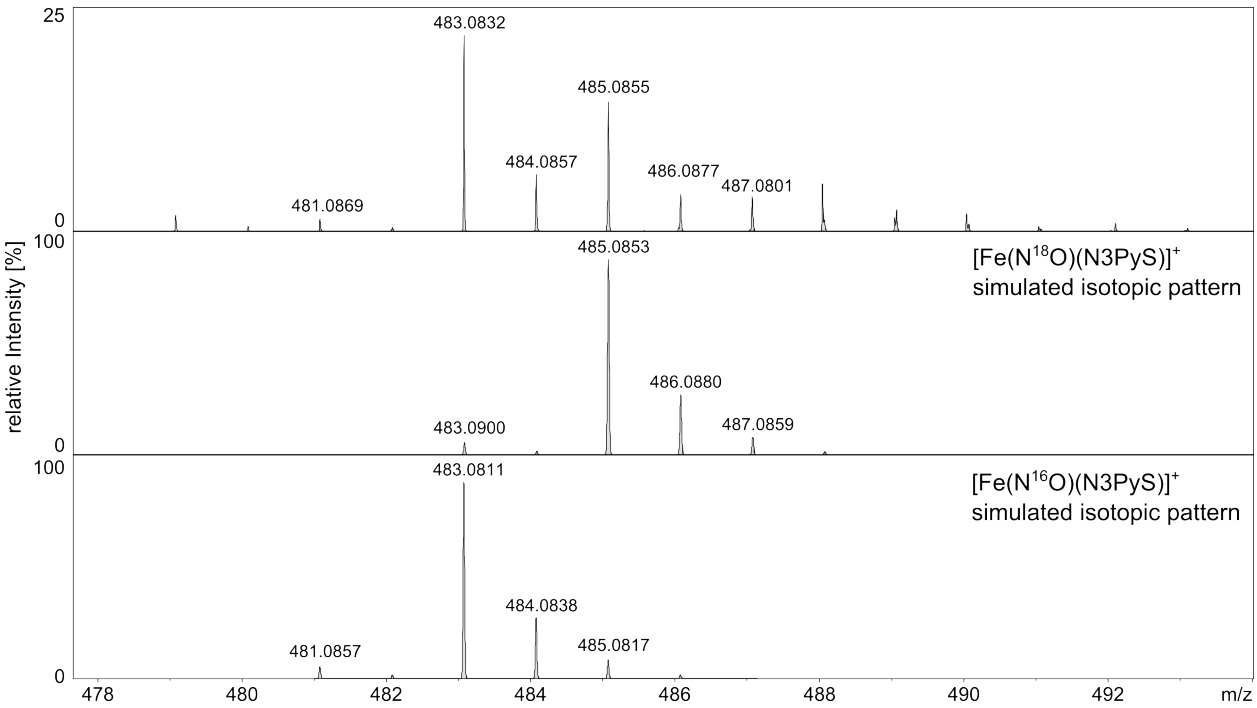

Figure S9. CSI-MS of a sample of **2** + $^{18}O_2$ in CH_3CN after 25 min of photoirradiation (150 W xenon lamp: $\lambda > 400$ nm) (top spectrum) showing the peaks corresponding to $[Fe(N^{18}O)(N3PyS)]^+$ (simulated isotope pattern, middle spectrum) and to $[Fe(N^{16}O)(N3PyS)]^+$ (simulated isotope pattern, bottom spectrum).

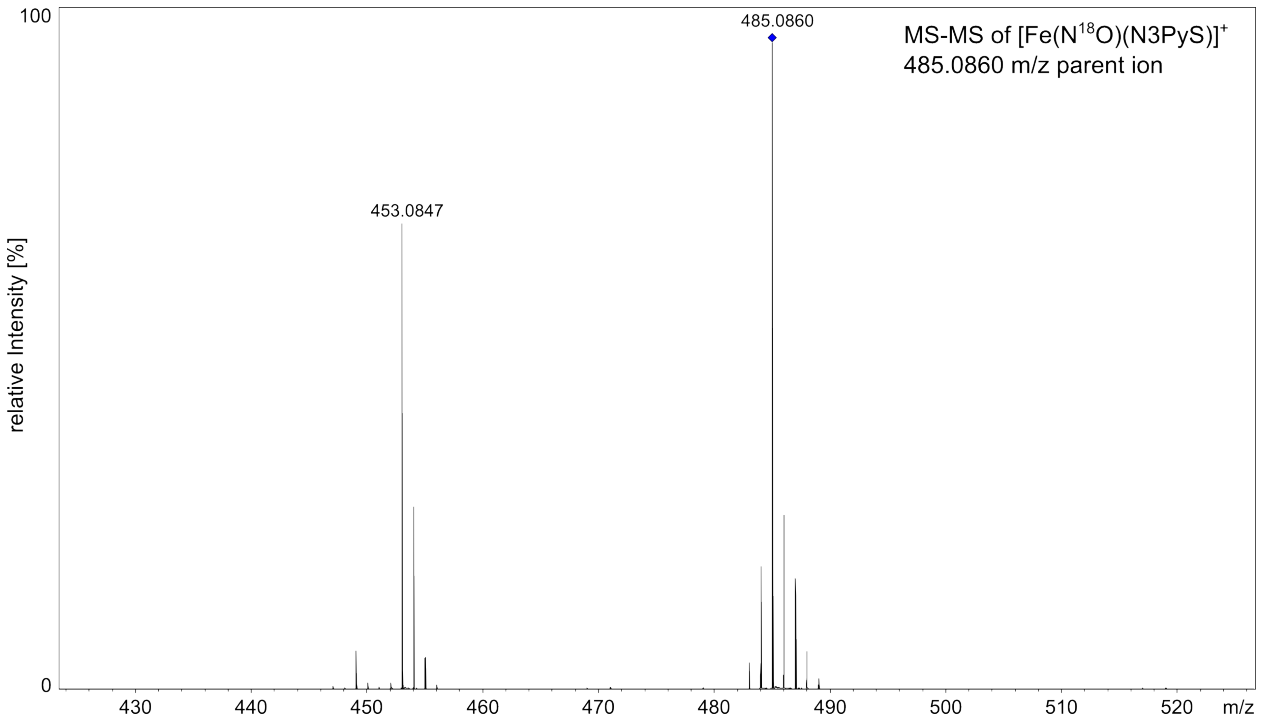

Figure S10. Tandem MS/MS of the parent ion at 485.0860 m/z generated from the reaction of **2** + $^{18}O_2$ in CH_3CN after 25 min of photoirradiation showing the loss of $N^{18}O$• to give $[Fe^{II}(N3PyS)]^+$ at 453.0847 m/z.

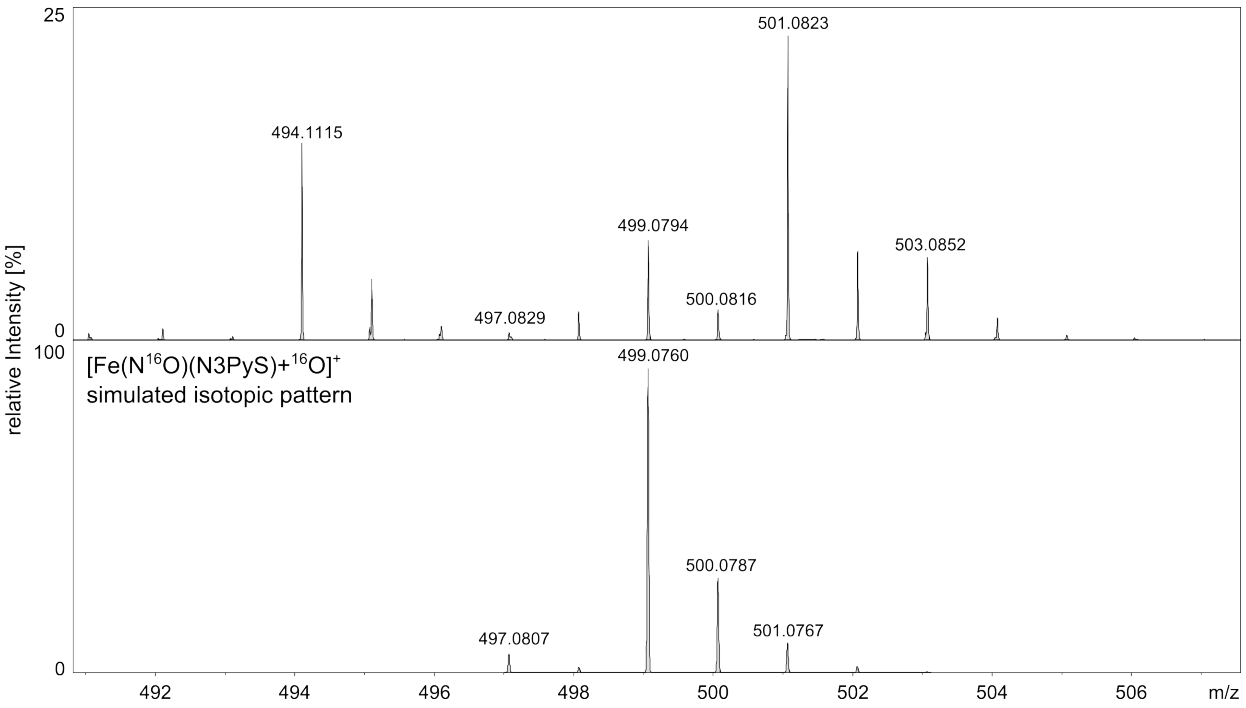

Figure S11. CSI-MS of a sample of **2** + $^{18}O_2$ in CH_3CN after 25 min of photoirradiation (150 W xenon lamp: $\lambda > 400$ nm) (top spectrum) with the simulated isotope pattern corresponding to $[Fe(N^{16}O)(N3PyS)+^{16}O]^+$ (bottom spectrum).

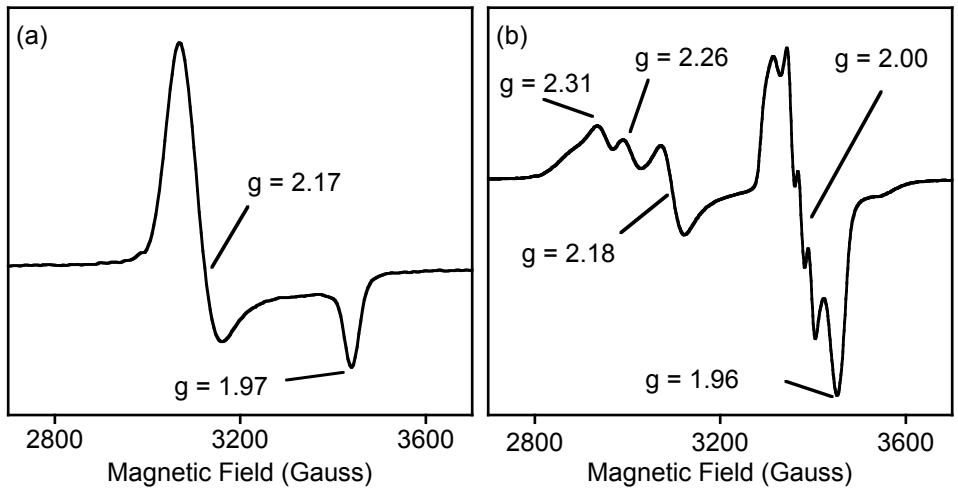

Figure S12. EPR spectra (12 K, 1.8 mM in toluene/CH_3CN) of (a) the one-electron oxidized $[Fe^{III}(N3PyS)(CH_3CN)]^{2+}$ and (b) $[Fe^{III}(NO_2)(N3PyS)]^+$ (**4**) generated via pathway B.

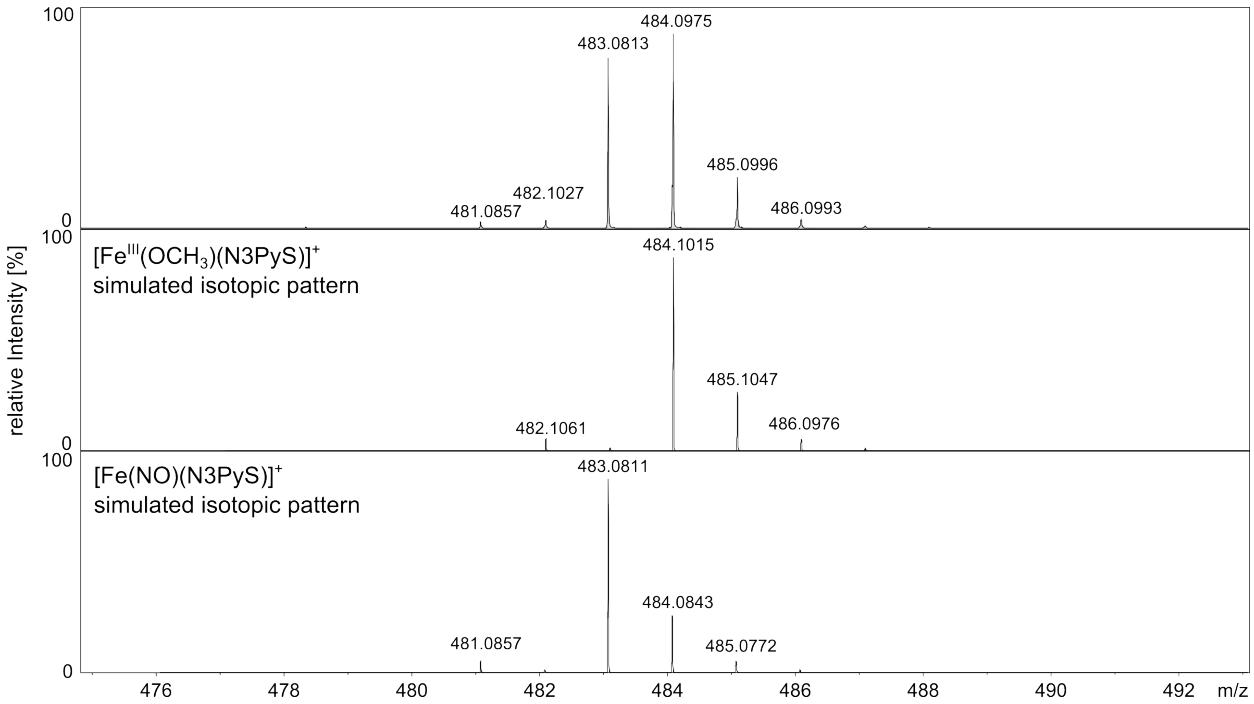

Figure S13. CSI-MS of **2** dissolved in MeOH prior to photoirradiation (top spectrum) with simulated isotope patterns corresponding to $[Fe^{III}(OCH_3)(N3PyS)]^+$ (middle spectrum) and $[Fe(NO)(N3PyS)]^+$ (bottom spectrum).

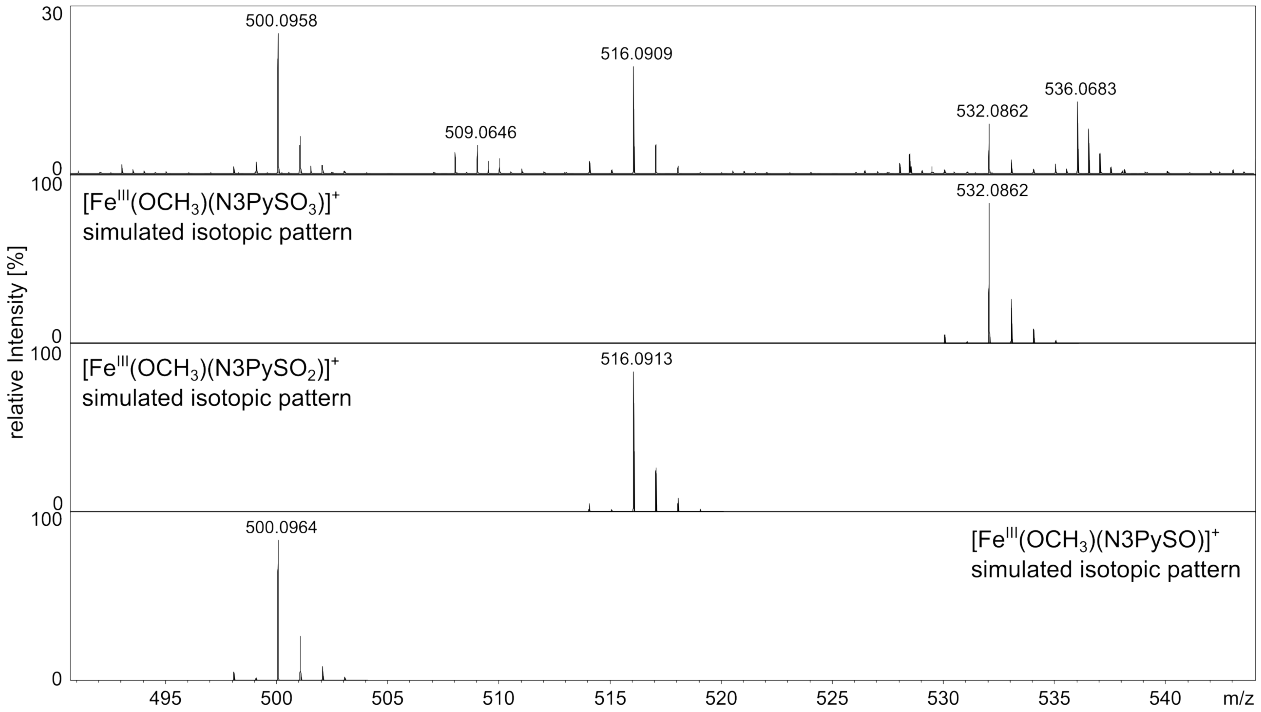

Figure S14. CSI-MS of the reaction of **2** + O_2 in MeOH after 20 min of photoirradiation (150 W xenon lamp: $\lambda > 400$ nm) (top spectrum) with the simulated isotope patterns corresponding to $[Fe^{III}(OCH_3)(N3PySO_3)]^+$ (second spectrum), $[Fe^{III}(OCH_3)(N3PySO_2)]^+$ (third spectrum), and to $[Fe^{III}(OCH_3)(N3PySO)]^+$ (bottom spectrum).

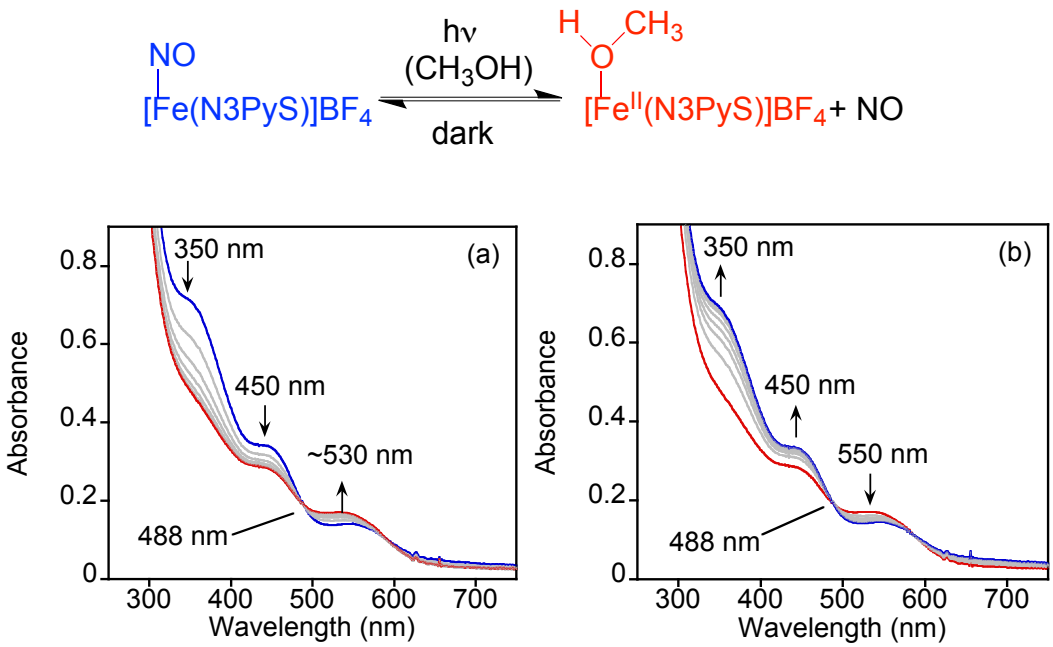

Figure S15. Reversible dissociation of nitric oxide for **2** under air-free conditions in CH_3OH (top). Time-resolved UV-vis spectra showing (a) the release of NO• from **2** upon continuous irradiation ($\lambda > 400$ nm) in CH_3OH (0 – 25 min) and (b) the rebinding of NO• to **1** in CH_3OH in the dark (0 – 4 h).